Modified Excitation Signals for AMB Identification Procedures

Diego Diaz[1], Fernando Pinto[2], Thiago Ritto[3], David Maldonado[4], and Vinicius Côrtes[5]

[1] Acoustics and Vibrations Laboratory, Federal University of Rio de Janeiro, Brazil
dgodoy@ufrj.br
[2] fcpinto@ufrj.br
[3] tritto@mecanica.ufrj.br
[4] davidjuliang@hotmail.com
[5] viniciuscortes@poli.ufrj.br

Abstract

In this paper modified signals obtained by means of an optimization algorithm are used for identification procedures in a previous developed small-scale active magnetic bearing (AMB) test rig. Such an iterative algorithm reduces the crest factor of the original signal allowing higher energy injection into the system, yielding a higher signal-to-noise ratio if compared with general broadband excitation signals (swept, white noise, impulse, etc.). The results are compared with the well known stepped sine, which has the ability to concentrate the energy in a unique desired frequency, however at the cost of a significant increase of the total experiment time.

1 Introduction

The choice of excitation signals is an important step when an identification procedure, or a sensitivity analysis, is the scope of any system under test, even more when the allowed time to perform the experiment is a constrain. The bandwidth and its energy distribution are the most common aspects to have into account for an optimal excitation signal design. Due to the inherent presence of noise in experimental measurements, some strategies may be implemented aiming to increase the signal to noise ratio (SNR), and thus obtain more accurate estimations[9]. In the case of magnetic bearing systems, as well as various applications, the excitation signal amplitude is restricted by the maximum shaft displacement, namely, a part of the gap between the rotor and the touchdown bearing. A straightforward way, which consists in a longer experiment time to perform averaging techniques with a higher number of repetitions, as studied in detail by Verboben [21], may not be effective when the test stand is not able to maintain the test conditions for a long period, for instance, high pressure and flow ratio test rigs in oil and gas applications. In such a scenario, the study and assessment of different excitation signals become an interesting alternative to obtain a *balanced* solution between the time and amplitude restrictions.

In previous works, various excitation signals have been used in active magnetic bearing systems (AMBs) aiming a comparison of each signal performance. Perhaps the experiments developed by Hynynen [7] were the first to highlight the importance of well-designed signals for identification of an AMB test rig transfer function. In the same way, Khader et. al. [8] performed a similar analysis in order to assess different averaging methods, or also known in literature as *estimators* [5]. Multitone signals were tested in a high pressure test chamber devised by General Electric turbomachinery manufacturer [20] to evaluate the behavior of annular gas seals in presence of pressurized nitrogen. A reduction of total experiment time was one of

the most important remarks in that paper. A qualitative comparison of the obtained frequency response functions (FRFs) by utilizing several excitation signals was performed by Vuojolainen et al. [22]. Likewise, Diaz et al. [2] obtained the FRFs of a small-scale AMB test rig by using different averaging methods in a non-rotating shaft condition and then at several rotation speeds [3]. With the addition of modified multitone excitation signals, the latter authors performed [4] an estimation of the equivalent stiffness and damping coefficients of the same AMB test rig, observing the benefits when the crest factor of an excitation signal is reduced, resulting in lower uncertainties.

A comparison between pure harmonic, broadband general purpose and modified excitation signals are performed in a small-scale AMB by applying the method utilized in[4], and presenting the results in a relative instead an absolute approach, which gives a better understanding of the uncertainties behavior of the different excitation signals applied to the test rig.

2 Identification Procedure

Due to the robust performance in presence of noise [19], identification method is made on the frequency domain approach, i.e. the use of frequency response functions (FRFs). The excitation signal $\mathbf{s}$ is summed to the control signal (see Figure 1) while the rotor is levitating. Both the excitation, current and position signals are measured, conditioned and stored in an acquisition system, represented by $\mathbf{u}$ for the currents and $\mathbf{y}$ for the shaft position vectors. Those vectors are composed by their respective *true* values ($\mathbf{u_0}$ and $\mathbf{y_0}$) and also by the noise contribution vectors ($\mathbf{n_u}$ and $\mathbf{n_y}$). The noise effect are considered to be independent for each sensor and has the proprieties of a normally distributed random variable. Then the Discrete Fourier Transform (DFT) technique is applied to those stored signals in order to obtain their spectrum. Finally, the ratio of the output to the input signal (excitation) can be defined as the FRF of the system.

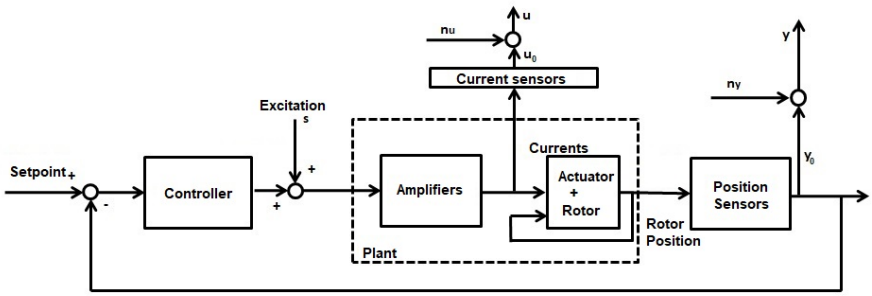

Figure 1: Block diagram for AMB identification (adapted from [17])

2.1 Identification Model

A two DOF mass-spring-damper model is employed to obtain the coefficients from the measured data. The tests are carried out with at rest condition (non-rotating shaft), and the governing equation can be represented as [23]:

$$\boldsymbol{M}\ddot{\mathbf{q}} + \boldsymbol{C}\dot{\mathbf{q}} + \boldsymbol{K}\mathbf{q} = \mathbf{f}, \tag{1}$$

where the vectors $\mathbf{q} = \begin{bmatrix} x & y \end{bmatrix}^T$ and $\mathbf{f} = \begin{bmatrix} f_x & f_y \end{bmatrix}^T \in \mathbb{R}^{2\times 1}$ represent the displacements and forces applied to the system, respectively. Therefore, stiffness $\boldsymbol{K}$, damping $\boldsymbol{C}$ and mass $\boldsymbol{M}$ matrices are expressed as:

$$\boldsymbol{M} = \begin{bmatrix} m & 0 \\ 0 & m \end{bmatrix}, \boldsymbol{C} = \begin{bmatrix} C_{xx} & C_{xy} \\ C_{yx} & C_{yy} \end{bmatrix}, \boldsymbol{K} = \begin{bmatrix} K_{xx} & K_{xy} \\ K_{yx} & K_{yy} \end{bmatrix}, \in \mathbb{R}^{2\times 2}. \tag{2}$$

The subscripts xx, yy and xy, yx represent the direct and cross-coupled effect in the system, respectively. m is related to the body (i.e. rotor) mass. By replacing the current and position vectors into their complex form (i.e. $\mathbf{q} = \bar{\mathbf{q}}_\mathbf{u} e^{j\omega t}$ and $\mathbf{f} = \bar{\mathbf{f}}_\mathbf{u} e^{j\omega t}$), equation 1 can be expressed as follows[11]:

$$\underbrace{\left[\boldsymbol{K} - \omega^2 \boldsymbol{M} + j\omega \boldsymbol{C}\right]}_{CDS} \bar{\mathbf{q}}_\mathbf{u} = \boldsymbol{H} \bar{\mathbf{q}}_\mathbf{u} = \bar{\mathbf{f}}_\mathbf{u}, \tag{3}$$

with $\boldsymbol{H} \in \mathbb{C}^{2\times 2}$ denoting the complex dynamic stiffness (CDS) of the system, $j = \sqrt{-1}$ and ω the excitation frequency. The force vector depends on the measured coil currents, shaft position and actuator topology (number of poles, air gap, pole area, etc.). For the system under test, as described in section 4, the force can be computed by the linear equation[10]:

$$\mathbf{f} = \begin{bmatrix} f_x \\ f_y \end{bmatrix} = \underbrace{\frac{4\cos(\pi/8)\mu_0 A_g N_v^2 i_b}{g_0^2}}_{\boldsymbol{K}_{mag,i}} \begin{bmatrix} i_x \\ i_y \end{bmatrix} + \underbrace{\frac{-4\cos(\pi/8)\mu_0 A_g N_v^2 i_b^2}{g_0^3}}_{\boldsymbol{K}_{mag,x}} \begin{bmatrix} x \\ y \end{bmatrix}, \tag{4}$$

where μ_0 represents the permeability of free space, A_g the pole cross-sectional area, N_v the number of turns in each coil, g_0 the nominal magnetic airgap, i_b the base current and $\begin{bmatrix} i_x & i_y \end{bmatrix}^T$ the vector of the control currents. Note that at least two *different* experiments ($\bar{\boldsymbol{Q}} = \begin{bmatrix} \bar{\mathbf{q}}_{\mathbf{u1}} & \bar{\mathbf{q}}_{\mathbf{u2}} \end{bmatrix}^T$ $\bar{\boldsymbol{F}} = \begin{bmatrix} \bar{\mathbf{f}}_{\mathbf{u1}} & \bar{\mathbf{f}}_{\mathbf{u2}} \end{bmatrix}^T$)are required to obtain the CDS matrix, which finally is written as:

$$\boldsymbol{H} = \begin{bmatrix} K_{xx} - m\omega^2 + j\omega C_{xx} & K_{xy} + j\omega C_{xy} \\ K_{yx} + j\omega C_{yx} & K_{yy} - m\omega^2 + j\omega C_{yy} \end{bmatrix} = \bar{\boldsymbol{F}}\,\bar{\boldsymbol{Q}}^{-1}. \tag{5}$$

A typical way to obtain the two independent experiments is firstly apply only the excitation force on the x axis and then perform the second one applying the force on the y axis.

2.2 Estimator

Aiming to reduce the noise effect, various repetitions or *blocks*[14] are carried out, and averaging techniques are utilized to obtain the force and displacement matrix. Pintelon and Shouckens[13] describe in detail the proprieties of the averaging methods used in the frequency domain. For the analysis made in this paper, the *error in variables* estimator was selected, which for each excitation frequency ω_k and a defined number of blocks N_b, can be expressed as:

$$\boldsymbol{H}_{\boldsymbol{EIV}}(\omega_k) = \left(\frac{1}{N_b} \sum_{l=1}^{N_b} \bar{\boldsymbol{F}}(\omega_k)^{(l)} \right) \left(\frac{1}{N_b} \sum_{l=1}^{N_b} \bar{\boldsymbol{Q}}(\omega_k)^{(l)} \right)^{-1}. \tag{6}$$

3 Excitation Signals

The stepped sine, which has an amplitude A and can be expressed as $s_t = A\cos(\omega_k t)$, has a high SNR since the energy is stored in only the excited frequency [15], and is one of the common

excitation signals used in system identification procedures. Its major limitation lies in the total time needed to perform the experiment. On the other hand, some broadband signals, as the widely used sweep, impulse or white noise are a practical solution to tackle the time limitation issue. Nevertheless, such signals distribute the energy in a great quantity of frequencies, yielding a lower SNR. The linear swept signal can be defined as follows[14]:

$$s(t) = A\sin((at+b)t) \qquad 0 \leq t \leq T_0, \tag{7}$$

with $a = \pi(k_2 - k_1)f_0^2$ and $b = 2\pi k_1 f_0$, $f_1 = k_1 f_0$ and $f_2 = k_2 f_0$ and $f_0 = 1/T_0$. The random signals are generated by a computer algorithm, and are able to satisfy the noise theory proprieties. In this case, the common used *pseudo-white* noise is chosen to be one of the excitation signal for the comparison.

An intermediate alternative is related to *multisine* or *multitone* signals, which are defined as the sum of N_f number of discrete harmonics, and are capable to distribute the energy into the chosen frequencies. Such a signal can be represented as:

$$s(t) = \sum_{k=1}^{N_f} A_k \cos(\omega_k t + \phi_k), \tag{8}$$

3.1 Modified multisine signals

The shape of a multisine signal relies on the set of its amplitudes (A_k), frequencies (ω_k) and phases (ϕ_k) . Impulsive signals trend to allow a lower amount of energy into the system under test[15]. Such characteristic can be quantified by the crest factor, denoted as[14]:

$$Cr(u) = \frac{s_{pk}}{s_{rmse}} = \frac{\max\limits_{t\in[0,T]} |s(t)|}{s_{rms}\sqrt{P_{int}/P_{tot}}}, \tag{9}$$

where $s_{rms} = \sqrt{\frac{1}{N}\sum_{i=1}^{N} s_i^2}$ is the signal RMS, s_{pk} its peak value, P_{tot} and P_{int} are the total and the contained power in the frequency band of interest, respectively. In general words, the lower the crest factor, the less impulsive the signal is. A second indicator, known as time factor[14], indicates how long takes for each frequency component to have the same SNR when compared to a stepped signal with the same frequency.

There exist several techniques to reduce the crest factor by *manipulating* the signal phases, for instance, the equation proposed by Schroeder [16]. Some iterative algorithms, like the Chebyshev method[6], also have an effective performance. Such a method consists in an optimization problem, where the objective is the minimization of the cost function l_p, which is dependent of the $p-th$ norm of the signal excitation vector, yielding a lower crest factor. The algorithm flow chart can be observed in Figure 2. The phases can be initialized randomly, and then a Levenberg-Marquardt algorithm[12] is applied in order to update the set of phase values. As the crest factor converges, the $p-th$ norm is increased twice until a minimum possible Cr is obtained or the maximum defined $p-th$ is reached.

As an example, a multitone signal with 17 frequencies with flat spectrum (i.e. $A_1 = A_2 = ... = A_{17}$), is used to assess the optimization algorithm. The frequencies are selected to be evenly spaced and distributed following the expression $\omega_k = 2\pi(4k+1)$ with $k = 1, 2, ..., 17$. The spectrum of the original signal, as well as its last iteration step is presented in Figure 3. Note that the spectrum amplitudes are conserved whilst the phases are modified to reduce the peaks of the signal. The crest factor evolution can be observed in figure 4. The numbers located

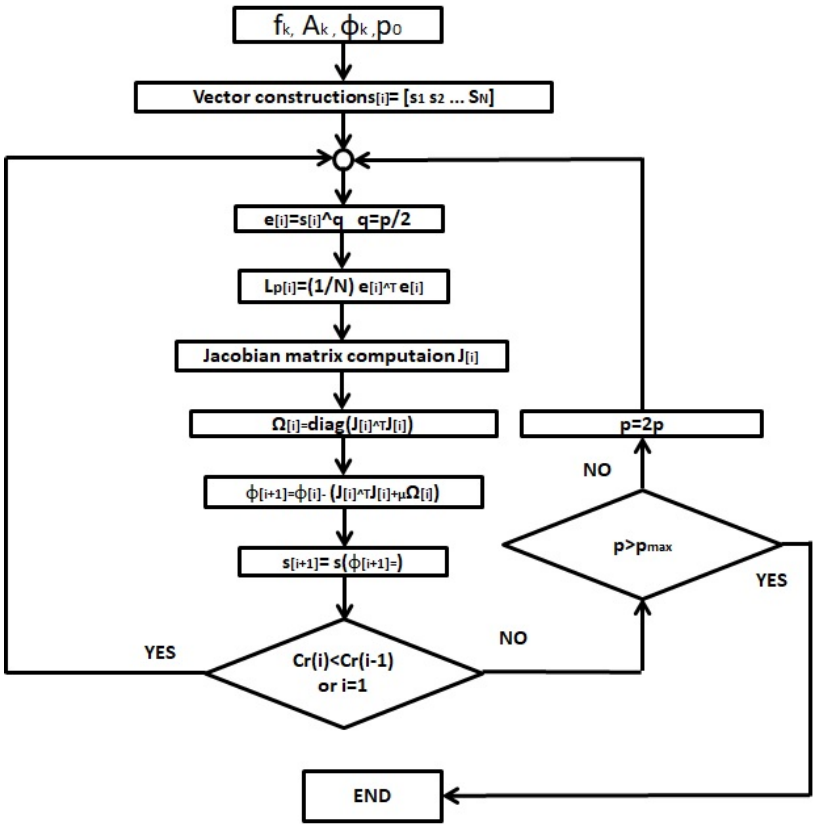

Figure 2: Chebyshev method flow chart [6]

close to some points of the curve indicate the $p-th$ norm value and in which iteration they were increased by two. In this case, the lowest possible crest factor was 1.61, and the algorithm took 73 iterations to converge on the final value. The lasted time was approximately 4 seconds, with a Matlab^{TM} script and a computer with basic specifications (Intel®core i5^{TM} and 8 GB of RAM).

3.2 Experiment time

The total demanded time to perform the data acquisition, in a defined frequency band, when a stepped signal is used [15], can be estimated by using the equation:

$$T_{step} = N_e \left(N_f \left[T_w + N_b \sum_{i=0}^{N_f - 1} \left(\frac{1}{f_i} \right) \right] \right), \tag{10}$$

where T_w refers to the needed time to leave the transient effect when the frequency is modified, and N_e are the number of independent experiments to be performed (for this case, as mentioned in subsection 2.1, $N_e = 2$). In the same way, a time needed to acquire the data, within the

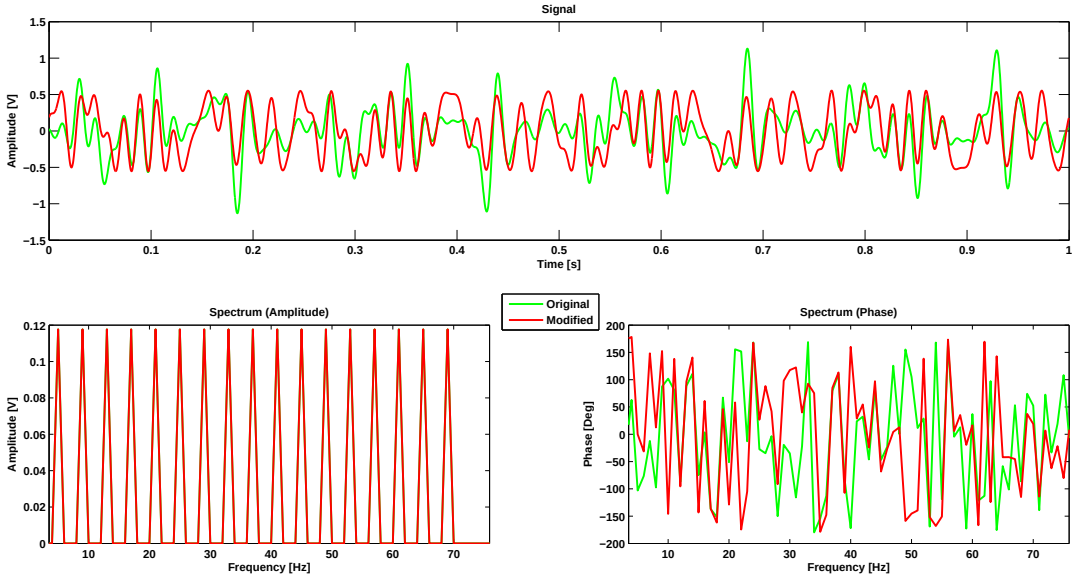

Figure 3: Original and modified multisine signal with Chebyshev method

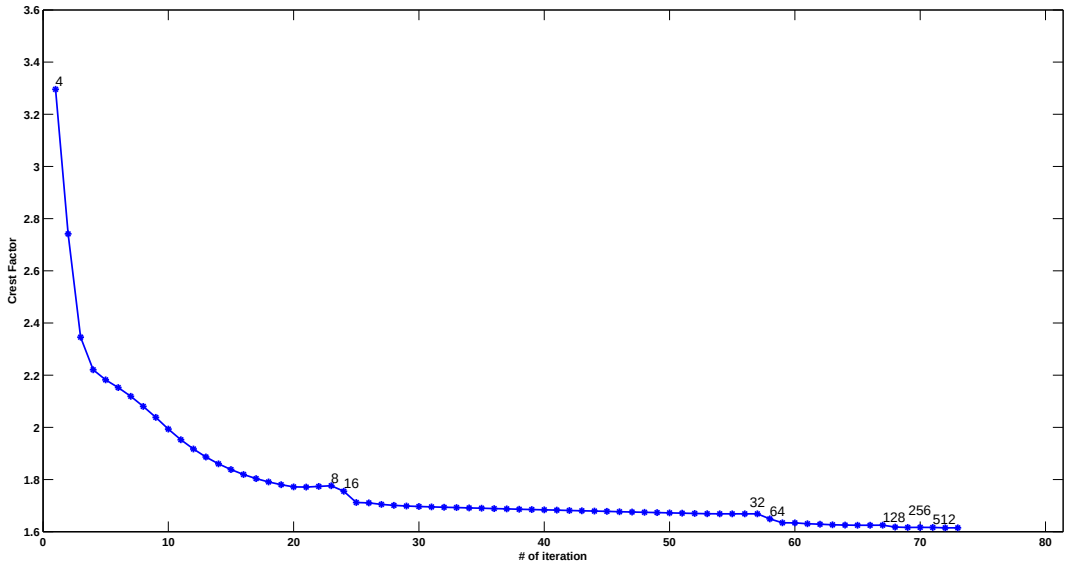

Figure 4: Crest factor evolution for signal presented in Figure 3

same frequency band, when a multisine signal is used, can be calculated by[15]:

$$T_{ms} = N_e \left(\frac{N_b}{f_0} + T_w \right), \tag{11}$$

with f_0 the lowest frequency excited value.

4 Small Scale AMB Test Rig

A rigid rotor supported by an active magnetic bearing system, previously developed in the Acoustics and Vibrations Laboratory [1][18] at Federal University of Rio de Janeiro, was used to assess the excitation signals for the identification procedure, which comprises the estimation of the equivalent AMB stiffness and damping coefficients. Such a test rig can be observed in Figure 5. Each magnetic actuator has an eight heteropolar *coupled pair* configuration. To levitate the rotor, it was employed a closed loop decentralized PID control algorithm, implemented in a development FPGA module by means of the Tustin approximation, with a discrete control period of $100\mu s$. Furthermore, a differential mode is adopted to reduce the complexity of the control strategy scheme. The algorithm also allows to add the excitation signals after the control block output as shown in Figure 1. The main dimensional and functional characteristics are summarized in Table 1.

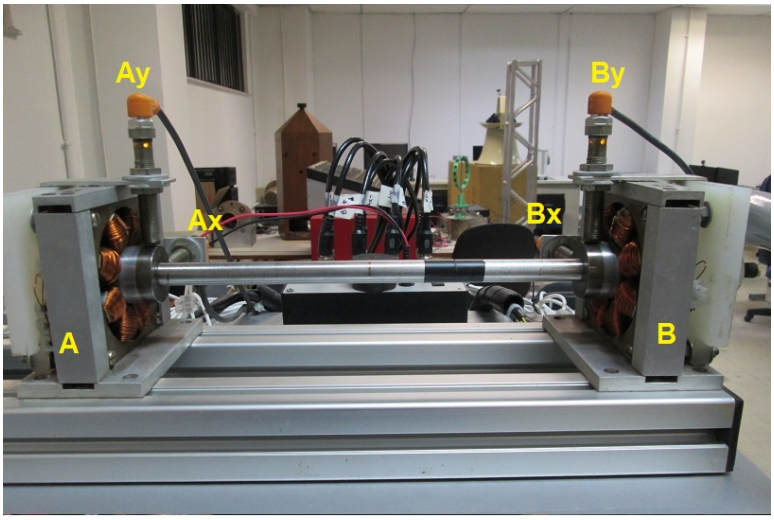

Figure 5: Small scale AMB test rig used for experiments

Because the identification model structure is governed by only lateral displacements, both sides A and B are excited in the same way to mimic only translational motion. Then the measurements are obtained from the both side sensors, and averaged to obtain the resulting displacement data. Therefore, the magnetic forces from the actuator A and B are summed to compute the resultant system force.

5 Results

For the experiments, it was selected a total of six excitation signals (see Table 2), comprised of the widely used stepped sine, white noise, sweep and the last three are composed of multisine signals. The first one of that latter group has the phases obtained randomly within an interval $\begin{bmatrix} 0 & 2\pi \end{bmatrix}$ with a uniform distribution, and the spectrum shape adjusted in such a way that the

Parameter	Symbol	Value	Unit
Shaft mass	m	1	kg
Shaft length	L_s	400	mm
Shaft diameter	d_s	14.28	mm
Journal diameter	d_j	36.4	mm
Touchdown bearing diameter	d_{to}	1	mm
Distance between actuators	$2a$	330	mm
Distance between sensors	$2c$	315	mm
Number of turns per pole	N_v	130	
Bias current	i_b	1	A
Flux density saturation	B_{sat}	1.7	T
Nominal radial airgap	g_0	1	mm
Pole cross-sectional area	A_g	235	mm^2
Open-loop gain	$K_{mag,x}$	-2.11e4	Nm^{-1}
Actuator gain	$K_{mag,i}$	21.14	NA^{-1}
Nominal inductance	L_0	4.3	mH
Coil wire gauge		20	AWG
Number of poles per actuator	N_p	8	

Table 1: Small AMB test rig characteristics

frequencies that require more energy, have their respective input amplitudes increased aiming to maintain the output spectrum amplitude flat. For inductive loads as magnetic bearing applications, this occurs at higher frequencies. To obtain the spectrum shape, the FRF amplitude of the AMB system can be obtained by utilizing any broadband excitation signal, considering the ratio of the input to the displacement spectrum amplitude. Since the objective is to know only the amplitude, it is not required many blocks, indeed, one block should be sufficient. With the same spectrum amplitude shape, the second multisine signal has its phases optimized by the l_p algorithm (i.e. Chebyshev method), and finally, the last multitone signal also has its phases optimized, but instead adapted amplitudes, its shape consists of a flat spectrum. The band of

	Signal	Spectrum amplitudes	Spectrum phases
1	Stepped Sine	Adapted	-
2	Sweep	Flat	-
3	White noise	-	-
4	Modified multisine with l_p algorithm	Flat	Optimized
5	Multisine with random phases	Adapted	Random
6	Modified multisine with l_p algorithm	Adapted	Optimized

Table 2: Excitation signal characteristics

interest was defined well below the maximum force slew rate, starting in 5 Hz with 17 components. In order to separate the nonlinear distortions, at least, the fourth order contribution, the $k-th$ frequency follows the expression $\omega_k = 2\pi(4k+1)$.

A dedicated acquisition module, which stores synchronously the excitation signals, currents and positions measurements from the AMB is used at the rate of $5kHz$. As an example, a period of the excitation signal *6-Modified multisine with l_p algorithm*, when the x axis is excited, as well as its resulting force and shaft position can be observed in Figure 6. The

maximum displacement is set to not be more than $\pm 100\mu m$ from the center for all cases.

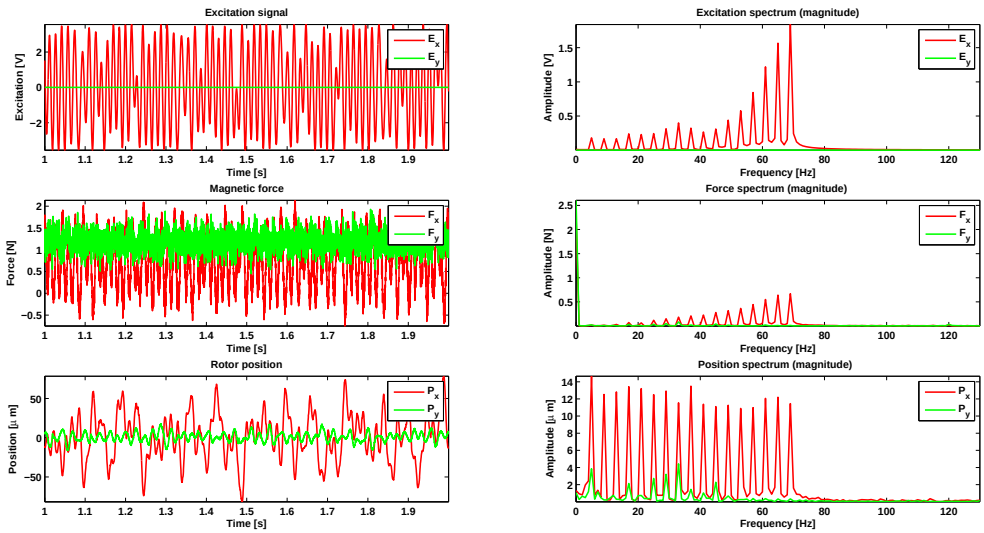

Figure 6: Excitation signal, force and shaft position for the signal *6-Modified multisine with l_p algorithm*, when axis x is excited

With an established number of blocks $N_b = 10$, the estimated stiffness coefficients are presented in Figure 7. Note that for the direct terms (i.e. K_{xx} and K_{yy}), all the values are close due to the contribution of the known mass and excitation frequency $m\omega^2$ (see Equation 5). The cross-coupled terms exist due the nonlinear magnetic actuator and its dependence of the shaft position rotor, and also the gravity contribution. The estimated damping coefficients can be observed in Figure 8. In general, the direct terms as well as cross-coupled damping terms seem to have no well defined pattern, and the estimated coefficients differences are more evident.

In order to analyze the uncertainties, the relative standard deviation concept is applied to the results presented previously in Figures 7 and 8, taking as reference the mean coefficient estimated in each frequency. For the stiffness and damping coefficients, as shown in Figure 9 and 10, respectively, the relative standard deviation curves confirm the outstanding performance of the stepped signal, which for almost all frequencies, had the lowest standard deviation. At low components (e.g. $5Hz$), it is possible to notice an increment of uncertainties, mainly in the direct terms of stiffness and damping, probably due to the low amplitude excitation signal required to move the shaft below the maximum allowed displacement, combined with the noise of the current sensors. There are several points obtained with the white noise and sweep signal that are not plotted in the figures, since they are located out of the graphic scale. Moreover, the signals with flat spectrum trend to have a higher standard deviation values at high frequencies, as expected, since the applied energy yields a lower system excitation in such frequencies. One can also observe the higher deviation in the x axis, associated likely to the gravity effect when the horizontal axis (i.e. x) is excited.

Aiming to have an overall sight of the assessed excitation signals, an average of the deviations over the band of interest is calculated for each term, and summarized in Table 3. It is possible to

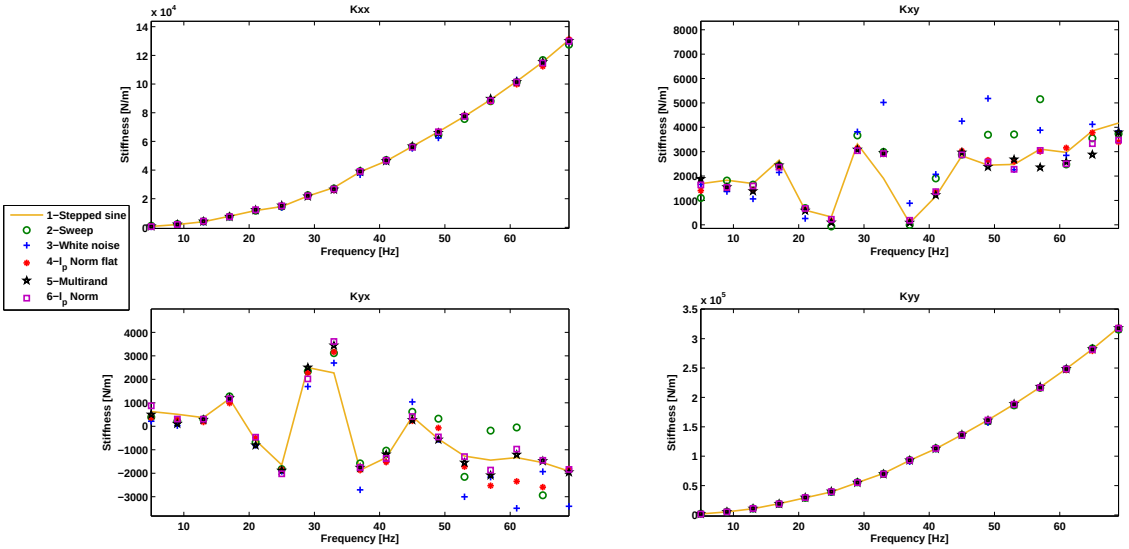

Figure 7: AMB estimated stiffness coefficients

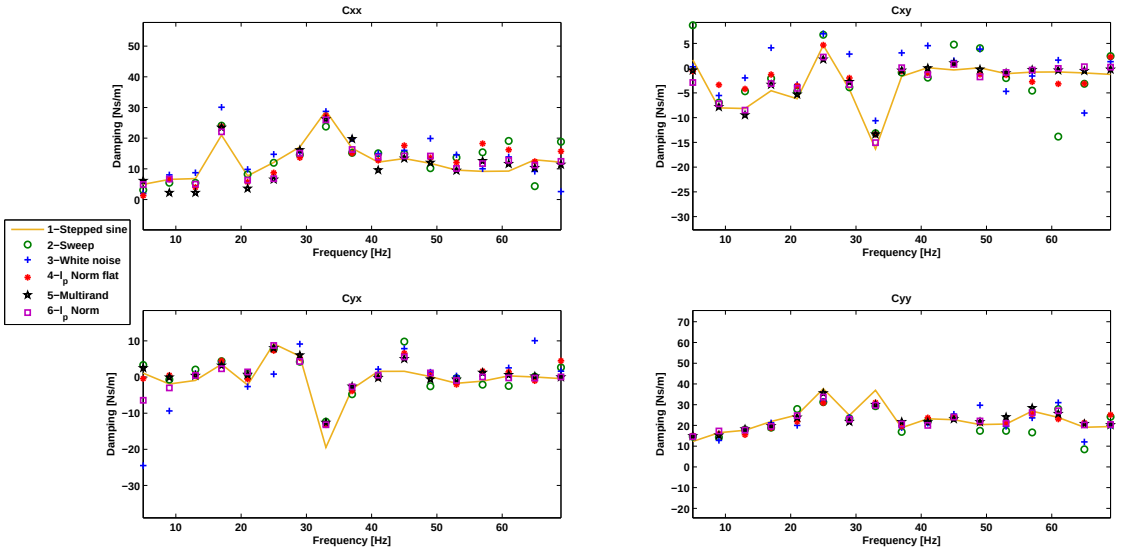

Figure 8: AMB estimated damping coefficients

observe the significantly lower deviation in multisine signals, if compared with sweep and white noise. The multitone signals with their phases modified by the Chebyshev method performed better than the multisine with random phases.

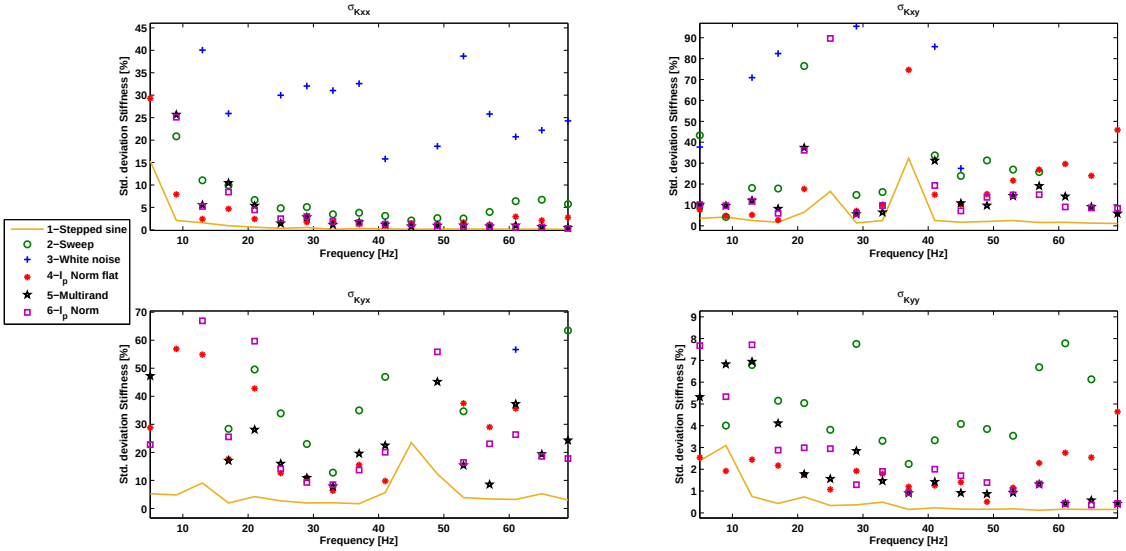

Figure 9: Relative standard deviation of the estimated AMB system stiffness coefficients

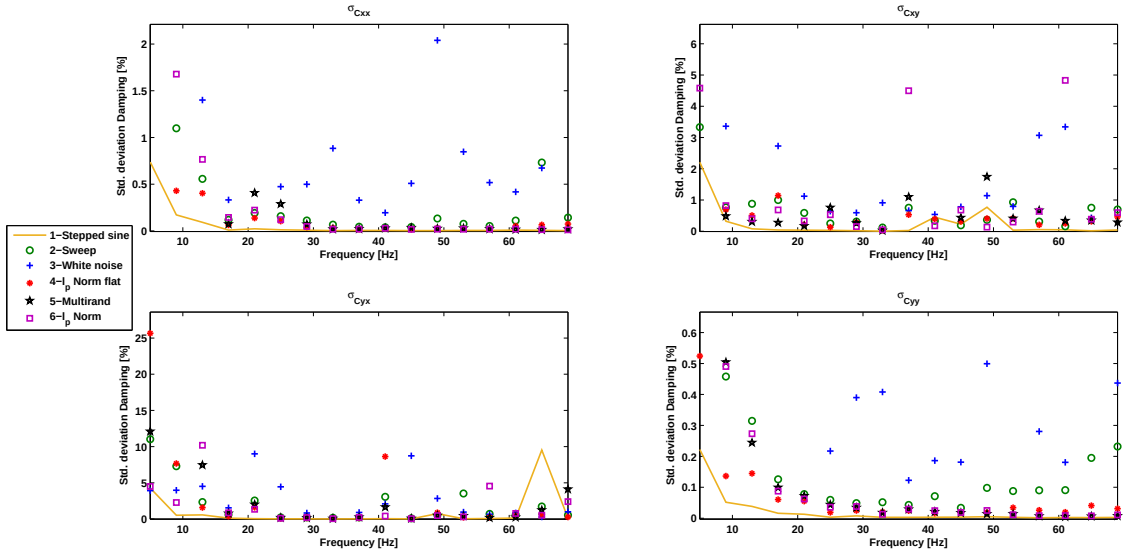

Figure 10: Relative standard deviation of the estimated AMB system damping coefficients

Because this paper intends not only to assess the uncertainties, but also the error with respect to the *true* values, a comparison of the estimated coefficients is carried out. The stepped sine, which had the lowest relative standard deviation, is chosen as the reference to

Excitation signal	σ_{Kxx} %	σ_{Kxy} %	σ_{Kyx} %	σ_{Kyy} %	σ_{Cxx} %	σ_{Cxy} %	σ_{Cyx} %	σ_{Cyy} %
1- Stepped sine	1.36	5.04	5.51	0.59	0.06	0.25	0.95	0.02
2- Sweep	21.99	223.84	606.30	6.44	0.68	0.68	2.08	0.36
3- White noise	76.24	519.60	253.91	28.03	1.66	7.81	15.94	1.11
4- Multisine (l_p) flat shape	3.94	24.47	74.08	1.96	0.56	1.48	2.86	0.07
5- Multisine with random phases	8.07	40.37	47.74	2.26	0.82	35.88	12.34	0.19
6- Multisine (l_p) adapted shape	7.58	23.59	33.57	2.49	0.69	1.16	1.71	0.15

Table 3: Relative standard deviation average for stiffness and damping coefficients, $N_b = 10$

calculate the relative error of the estimated stiffness and damping coefficients with the other five signals, presented in Figures 11 for stiffness and 12 for damping. The multitone signals obtained a lower error trend, when compared with the white noise and swept signals. It is also possible to observe a lower error at high frequencies for multisines with adapted spectrum amplitude than the obtained with flat amplitude signals.

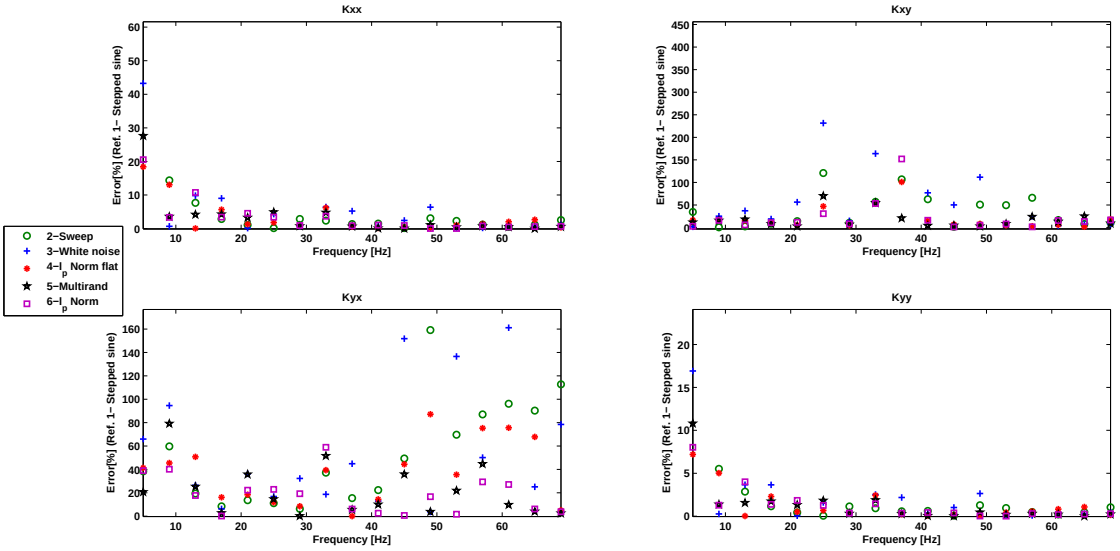

Figure 11: Relative error of the AMB estimated stiffness coefficients

As previously proposed for uncertainties, a general interpretation can be achieved by computing the mean relative error coefficients in the band of interest, which is summarized in Table 4. The Multisine signal with optimized phases and adapted spectrum shape presented the lowest errors (principally in the direct damping terms), with the exception of the cross-coupled damping C_{xy} and C_{yx}.

For the $N_f = 17$ frequencies, the total experiment times, which can be obtained by using Equation 10 for the stepped sine, and Equation 11 for the selected multisines (as well for white noise and sweep), where approximately 40 minutes and 40 seconds, respectively, meaning a ratio of 60 times. One can imply that the higher the number of frequencies, the greater the

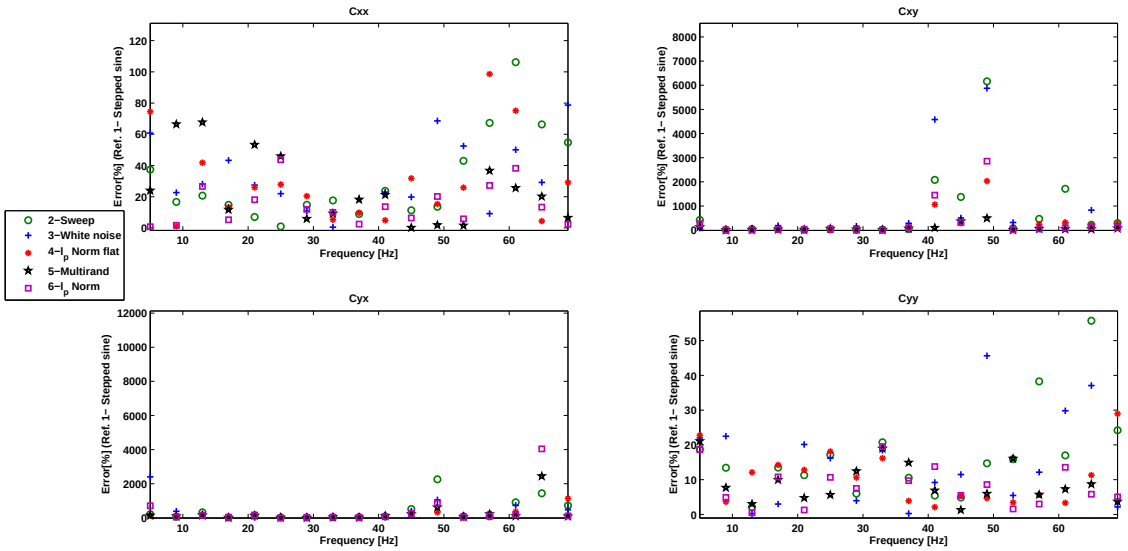

Figure 12: Relative error of the AMB estimated damping coefficients

Excitation signal	$\hat{Kxx}$	$\hat{Kxy}$	$\hat{Kyx}$	$\hat{Kyy}$	$\hat{Cxx}$	$\hat{Cxy}$	$\hat{Cyx}$	$\hat{Cyy}$
	%	%	%	%	%	%	%	%
2- Sweep	7.42	36.63	52.72	2.90	30.89	769.39	410.20	17.03
3- White noise	5.44	114.38	56.58	2.14	33.24	805.37	8446.3	15.27
4- Multisine (l_p) flat shape	3.29	19.80	37.46	1.29	29.69	292.95	1014.6	10.54
5- Multisine with random phases	3.37	17.70	21.63	1.31	24.46	92.24	259.81	9.06
6- Multisine (l_p) adapted shape	3.29	11.81	18.48	1.28	14.56	328.11	402.22	8.26

Table 4: Relative error deviation average for stiffness and damping coefficients, $N_b = 10$ Ref. 1- Stepped signal

total time experiment difference between the stepped and broadband excitation signal, however the lower the latter signal crest and time factor.

6 Conclusions and Future Works

Basically, the general purpose signals (sweep and white noise) performance were lower than multisines in the defined set of frequencies. In the case of white noise, it could be due to its energy distribution out of the frequencies of interest, thus yielding a reduction of applied power to the *desired* harmonics. In general, the best performed excitation signal for the tests carried out in this paper was the multisine with adapted spectrum amplitude and modified phases by using the Chebyshev method.

The direct terms of uncertainties and errors values were lower in the y axis (see Tables 3 and 4) than x axis. Such behavior may be caused by the gravity contribution, which can be represented as a vector parallel to the y axis.

The need of adapted amplitudes becomes more indispensable when the system under test spectrum has a low flatness (e.g. flexible shaft supported by an AMB system), namely, the signal should excite with lower amplitudes the frequencies located close to the system resonances.

As a suggestion, the excitation signal design starts with the band of frequencies definition, as well as its number of frequencies to cover such band. Then, the system spectrum amplitude is obtained in order to establish its shape. This procedure can be achieved by using a general purpose broadband signal, and computing the FRF magnitude of the excitation signal to the system output (it should not use more than two blocks). Finally, a reduction of the crest factor is made by means of algorithms as the presented in this paper.

Since the spectrum shape was obtained manually before applying the crest factor reduction, the authors are currently working on a new strategy aiming to include this step in an automatized way. Furthermore, future experiments are intended to compare the number of excited frequencies N_f and blocks N_b, which are strongly related to the total experiment time and signal excitation quality (crest and time factors).

References

[1] Jefferson Coelho. Aspectos mecânicos de sistemas de mancais magnéticos. M.sc. dissertation, Universidade Federal do Rio de Janeiro, Rio de Janeiro, RJ, Brasil, 2016.

[2] Diego Diaz, Fernando Pinto, Thiago Ritto, and David Maldonado. Stepped sine and multisine signal excitation for identification in a small amb test rig. In *Proceedings of the 24th International Congress of Mechanical Engineering*, page 9, Curitiba, Brazil, 2017.

[3] Diego Diaz, Fernando Pinto, Thiago Ritto, David Maldonado, and Vinicius Côrtes. Nonparametric identification of a small amb test rig at several rotating speeds. In *Proceedings of the 16th International Symposium on Magnetic Bearings (ISMB 16)*, page 7, Beijing, China, 2018.

[4] Diego Diaz, Fernando Pinto, Thiago Ritto, David Maldonado, and Vinicius Côrtes. Comparison of different excitation signals in a rotordynamic system. In *Proceedings of the 25th International Congress of Mechanical Engineering COBEM*, page 10, Uberlandia, Brazil, 2019.

[5] Patrick Guillaume. Frequency response measurements of multivariable systems using nonlinear averaging techniques. *IEEE Transactions on Instrumentation and Measurement*, 47:796–800, 1998.

[6] Patrick Guillaume, Johan Schoukens, Rik Pintelon, and Istvin Kollar. Crest-factor minimization using nonlinear Chebyshev approximation methods. *IEEE Transactions on Instrumentation and Measurement*, 40(6):982–989, 1991.

[7] Katja Hynynen. *Broadband Excitation in the System Identification of Active Magnetic Bearing Rotor Systems*. Ph.D. thesis, Lappeenranta University of Technology, Lappeenranta, Finland, 2011.

[8] Shahbaz Khader, Bin Liu, and Johan Sjöberg. System identification of active magnetic bearing for commissioning. In *Proceedings of International Conference on Modelling, Identification and Control*, pages 289–294, Melbourne, Australia, 2014.

[9] Lennare Ljung. *System identification: Theory for User*. Prentice Hall, 1987.

[10] Eric Maslen. *Magnetic Bearings*. University of Virginia, UVA. Lecture Notes, 2000.

[11] A Muszynska. *Rotordynamics*. Mechanical Engineering. CRC Press, 2005.

[12] J Norton. *An Introduction to Identification*. Dover publications, 2009.

[13] Rik Pintelon and Johan Schoukens. Measurement of frequency response functions using periodic excitations, corrupted by correlated input/output errors. *IEEE Transactions on Instrumentation and Measurement*, 50:1753–1760, 2001.

[14] Rik Pintelon and Johan Schoukens. *System Identification. A Frequency Domain Approach*. Wiley, 2012.

[15] Johan Schoukens, Rik Pintelon, and Yves Rolain. Broadband versus stepped sine frf measurements. *IEEE Transactions on Instrumentation and Measurement*, 49:275–278, 2000.

[16] Manfred Schroeder. Synthesis of low-peak-factor signals and binary sequences with low autocorrelation (Corresp.). *IEEE Transactions on Information Theory*, 16(1):85–89, 1970.

[17] Gerhard Schweitzer and Eric Maslen. *Magnetic Bearings. Theory, Design and Application to Rotating Machinery*. Springer, 2009.

[18] Renan Siqueira. Projeto e implementação de um mancal magnético ativo com controle por modos deslizantes. M.sc. dissertation, Universidade Federal do Rio de Janeiro, Rio de Janeiro, RJ, Brasil, 2013.

[19] O. Turkay and A.G. Ulsoy. Frequency versus time domain parameter estimation: Application to a slot milling operation. *Mechanical Systems and Signal Processing*, 2(3):265–277, 1988.

[20] Giuseppe Vannini, Stefano Cioncolini, Vincenzo Calicchio, and Francesco Tedone. Development of a high pressure rotordynamic test rig for centrifugal compressors internal seals characterization. In *Proceedings of the Fortieth Turbomachinery Symposium*, pages 46–59, Houston, USA, 2011.

[21] Peter Verboben. *Frequency-Domain System Identification for Modal Analysis*. D.sc. thesis, Vrije Universiteit Brussel, Buxelas, Belgium, 2002.

[22] Jouni Vuojolainen, Niko Nevaranta, Rafal Jastrzebski, and Olli Pyrhönen. Comparison of excitation signals in active magnetic bearing system identification. *Modeling, Identification and Control (MIC)*, 38:11, 2017.

[23] Toshio Yamamoto and Yukio Ishida. *Linear and Nonlinear Rotordynamics: A Modern Treatment with Applications*. Wiley, 2001.